Ocean Sci. Discuss., 6, 2831–2859, 2009
www.ocean-sci-discuss.net/6/2831/2009/

Ocean Science Discussions

This discussion paper is/has been under review for the journal Ocean Science (OS).
Please refer to the corresponding final paper in OS if available.

Spatio-temporal complexity analysis of the sea surface temperature in the Philippines

Z. T. Botin[1], L. T. David[2], R. C. H. del Rosario[1,*], and L. Parrott[3]

[1]Institute of Mathematics, University of the Philippines Diliman, 1101 Quezon City, Philippines
[2]Marine Science Institute, University of the Philippines Diliman, 1101 Quezon City, Philippines
[3]Département de géographie, Université de Montréal, C.P. 6128 succursale centre-ville, Montréal, QC H3C 3JY, Canada
[*]currently at: Genome Institute of Singapore, 60 Biopolis Street, #02-01 Genome, Singapore

Received: 25 October 2009 – Accepted: 16 November 2009 – Published: 26 November 2009

Correspondence to: L. T. David (ltd_pawikan@yahoo.com)

Published by Copernicus Publications on behalf of the European Geosciences Union.

Abstract

A spatio-temporal complexity (STC) measure which has been previously used to analyze data from terrestrial ecosystems is employed to analyse 21 years of remotely sensed sea-surface temperature (SST) data from the Philippines. STC on the Philippine wide SST showed the monsoonal variability of the Philippine waters but did not show significant differences between El Niño, La Niña and normal years. The spatial domain was subsequently divided into six thermal regions computed via clustering of temperature means. The STC values of each thermal region showed variations corresponding to the monsoonal shifts – as well as – to ENSO events. STC characterized environmental heterogeneity over space and time has the potential to define limits of bio-regions. The same approach can be utilized for many long-term remotely sensed data.

1 Introduction

Temperature is a controlling factor in ocean systems. Anomalies in sea surface temperature (SST) have a wide range of effects on marine ecosystems including the decline in reef fish population (Pratchett et al., 2006) and coral disease outbreaks (Bruno et al., 2007). In the early 1990's links between SST and coral bleaching were proposed (Lesser et al., 1990; Glynn and D'Croz, 1990). Strong et al. (1996) subsequently successfully identified suspected areas of coral reef bleaching using satellite derived SST. Recently, Peñaflor et al. (2009) focused on the SST of the Coral Triangle (which spans eastern Indonesia, parts of Malaysia, the Philippines, Papua New Guinea, Timor Leste and the Solomon Islands) and highlighted the importance of investigating how SST has changed through space and time within this region.

Here, we explore the hypothesis that the spatio-temporal complexity of the SST signal can be linked to physical processes such as prevailing winds and weather systems and our objective is to characterize these dynamics. We also hypothesize that the

OSD

6, 2831–2859, 2009

characteristic SST dynamics of the region may affect ecological properties such as the resilience of a system to warming events. In particular, we assess the ability of a recently developed measure of spatio-temporal complexity (STC) to distinguish which areas are affected by ENSO events and to differentiate regions subjected to different oceanographic conditions. STC is a relatively new measure whose applications to remotely sensed data in the ocean sciences has yet to be demonstrated. If sufficiently sensitive, such a measure could ultimately serve as an indicator of impending change in the dynamics of SST, which might help to detect the onset of coral bleaching or other regime shifts in the marine ecosystem.

The measure we use is based on entropy measures arising from information theory. Entropy measures are standard tools for measuring complexity and have been used to measure species diversity (Nsakanda et al., 2007). The use of information based Shannon entropy was first used to measure species diversity in MacArthur (1955) and although is it one of the most popular methods to measure the structural complexity of an ecological system, it is not able to measure the complexity of the system's dynamics (Parrott, 2005). Other information-based measures (e.g., Shannon entropy, effective complexity and fluctuation complexity) have been applied to the analysis of temporal data (time series) or to spatial data but not to both types of data (Andrienko et al., 2000; Wackerbauer et al., 1994; Parrott et al., 2008). It is important to capture both space and time in complexity measures and Parrott (2005); Parrott et al. (2008) introduced STC for this purpose (Fig. 1). It was applied to simulated vegetation data to explore its potential in characterising ecological spatio-temporal dynamics (Parrott, 2005) and was successfully used to analyze repeat photography data for a temperate forest in Parrott et al. (2008). STC is based on Shannon entropy and is able to incorporate the three dimensional nature of space-time fluctuations. It can be applied to spatio-temporal data sets wherein the state of a two-dimensional spatial mosaic has been recorded at regular time intervals and it can distinguish between ordered and disordered, complex or patchy spatio-temporal distributions (Parrott et al., 2008). It is also able to detect spatio-temporal patterns such as space-time cycles (Parrott, 2005).

OSD

6, 2831–2859, 2009

In this paper, we apply the STC algorithm on the 4 km resolution SST data to study the dynamics of Philippine SST both in space and in time. We expect the complexity of SST dynamics to be different for El Niño, La Niña and normal years and for regions subject to different oceanographic conditions. K-means clustering was used to identify regions under different oceanographic conditions and the STC of each of these regions was calculated to see how well the STC measure detects changes over time and space. To aid in analyzing the composite STC plots of each region, empirical orthogonal functions (EOF) were employed on the STC of each region.

2 Methods

2.1 SST data

SST data are from 1985–2005 night-time observations of the Advanced Very High Resolution Radiometer (AVHRR) on board the National Oceanic and Atmospheric Administration (NOAA)'s Polar Orbiting Environmental Satellites (POES). The AVHRR-SST products are twice-weekly 50 km datasets specifically developed for the NOAA Coral Reef Watch. The 50 km resolution data has been recently refined to 4 km resolution by the AVHRR Pathfinder Project of the National Oceanographic Data Center (NODC) and the University of Miami's Rosenstiel School of Marine and Atmospheric Science (see National Oceanographic Data Center, 2008). This 4 km SST data was used for the analysis and has a temporal resolution of once a week. The Philippine 4 km data was taken from the global data at location 114 to 130 longitude and 4 to 21.5 latitude. The resulting spatial dimensions of the SST matrix is 399 × 365 pixels, out of which the Philippine land mass occupies about 10% and its temporal dimension is 1092 (52 weeks × 21 years).

OSD
6, 2831–2859, 2009

2.2 Measuring spatio-temporal complexity

STC analyzes data consisting of $N_L \times N_W$ spatial points taken over a period of N_T time intervals and works particularly well for digital images of a rectangular area taken over time. The STC algorithm we use here works only with binary data, i.e., each spatial point or pixel can either be 1 or 0 (black or white). To convert the data to binary format, a threshold is chosen and each data point is converted to either 1 if its value is higher than the threshold, or it is converted to 0 otherwise. The choice of a threshold value is a key parameter in STC calculations and should be done as to ensure that a sufficiently high density of points is retained, while at the same time capturing the underlying dynamics. For data that is stationary in the mean and variance, the mean value is usually a good choice. For the Philippine SST data, the large fluctuations in temperature after the 1991 Mt. Pinatubo eruption gave rise to unusually high variance in the latter years of the dataset. For this reason, we chose to use the average temperature for the pre-eruption years (1985–1990) as our threshold. The computed average temperature was 25.1646°C.

After converting the data to binary, it is stacked into a 3-D $N_L \times N_W \times N_T$ matrix, and a "moving cube" is made to traverse the matrix while counting the number of non-zero entries (within the cube) at each position (see Fig. 1). The dimension n of this cube is taken to be much smaller than the dimensions of the data matrix (i.e., $n \ll N_L, N_W, N_T$) and the total number of possible positions of the cube inside the data matrix is $M = (N_L - n + 1) \cdot (N_W - n + 1) \cdot (N_T - n + 1)$. At each position of the moving cube, the number of non-zero entries (or the occupancy level) is denoted by $m_i, i = 1, \ldots, M$, and we tabulate the number of times the occupancy level m_i appears. Specifically, for an occupancy level of k, we count the number of m_i such that $m_i = k$ and denote this as μ_k. The relative frequency of k non-zero entries, denoted by p_k, is given by

$$p_k = \frac{\mu_k}{\mu_0 + \mu_1 + \ldots + \mu_{n^3}} , \quad (1)$$

OSD
6, 2831–2859, 2009

and the spatio-temporal complexity of the $N_L \times N_W \times N_T$ data matrix is given by

$$\mathrm{STC} = \frac{-\sum_{k=0}^{n^3} p_k \ln p_k}{\ln(n^3+1)} . \quad (2)$$

Here we impose that $\ln p_k = 0$ if $p_k = 0$.

The optimal use of STC in analyzing data is obtained by dividing the time dimension of the three-dimensional data matrix into slices and then computing the STC of this time slice. By plotting the STC value of this time slice with respect to time, the evolution of the system's spatio-temporal complexity is revealed. There are practical issues in choosing the thickness of the slices and in our implementation, we fixed the dimension of the moving cube to $n = 3$ ($3 \times 3 \times 3$ cube) and considered time slices consisting of 3, 4 or 5 consecutive time instances (i.e., STC is calculated for data matrices of $N_L \times N_W \times N_T$ weeks where $N_T = 3,4,5$). Furthermore, we also considered both non-overlapping and overlapping slices.

It is mathematically proven in Botin (2009) that STC gives the lowest value to a completely ordered 3-D data matrix and that it gives the highest value to a data matrix where all occupation levels are observed with equal frequencies. The highest value of STC thus corresponds to a spatio-temporal dynamics consisting of many frequent small patches and several large irregular patches that are constantly changing their sizes and locations in space and time. If we consider the patches as three-dimensional "blobs" in space-time, then the frequency distribution of blob volumes for a data matrix having an STC value of 1 follows a power law distribution (Parrott et al., 2008). On the other hand, a data matrix containing large sized and regularly shaped patches of non-zero entries would have high frequencies for fully occupied cubes and empty cubes and low frequencies for unempty cubes that are not fully occupied. Since this is closer to an ordered case, STC will assign a low value for this kind of data. Furthermore, Parrott (2005) discussed that unlike Shannon entropy which assigns the highest value to randomly generated data, STC assigns intermediate values for randomly generated

OSD
6, 2831–2859, 2009

binary 3-D matrices. Thus, according to the classification of complexity measures by Atmanspacher (2007), we can classify STC under the class of measures where complexity is a convex function of randomness.

High STC is thus of interest in a geophysical context, since it is an indication that the space-time dynamics of the variable studied has a scale-invariant, fractal structure, as typified by the power law distribution of blob sizes in the space-time matrix. Power-laws have been observed in many time series for physical systems and in spatial data, and fractal structures seem to be ubiquitous across many physical systems (Turcotte, 1997). In dynamical systems, the presence of power-law behaviour in space or time is a necessary but not sufficient condition for first order phase transitions and self-organized criticality (Bak and Chen, 1991; Goldenfeld, 1992; Reichl, 1998) and it is possible that this extends to spatiotemporal dynamics under regimes of high STC.

2.3 Identification of the thermal regions

To identify thermal regions with distinct temporal and spatial variability, we the obtained the average monthly temperature of each pixel/point of the of the spatial domain. A linear regression was done on each time series of monthly pixel values. Clustering (using k-means) was then performed to group regions with similar temporal dynamics. We followed the method in Peñaflor et al. (2009) and used the web-based geospatial clustering tool Deluxe Integrated System for Clustering Operations (DISCO) (Buddemeier et al., 2008) which can be accessed at http://fangorn.colby.edu/disco-devel/. The resulting regions are shown in Fig. 2 and are used in latter analysis.

2.4 Empirical orthogonal function analysis of the STC of each thermal region

The Empirical Orthogonal Functions (EOF) analysis used in oceanography is the same as Principal Component Analysis (PCA) and has also been called Proper Orthogonal Decomposition (POD) in reduced order modeling (Banks et al., 2002). EOFs provide the most efficient method of compressing data (Emery and Thomson, 2001; Banks

OSD
6, 2831–2859, 2009

et al., 2002) and the EOFs represent the uncorrelated modes of variability of the data (Emery and Thomson, 2001).

In oceanography, EOF is typically used to analyze data measured at different locations concurrently over a period of time. Here we consider the time histories of the STC of each thermal region during each chosen year (four representing normal years, three for El Niño years, three for La Niña years) and that they were measured concurrently during the same year. We then look for a set of orthogonal predictors or modes whose linear combination could account for the combined variance in all of the observations. Note that in EOF analysis, the data should be in the form of concurrent time-series records from a grid of recording stations but there are two difficulties with our STC data: (i) there are STC measurements taken at the same location (i.e., 10 yearly STC time histories for each thermal region), and (ii) the measurements are not taken in one year but during different years.

Let $S_j(t_i)$, $j = 1,\ldots,M$, $i = 1,\ldots,N$ be the yearly STC of the regions, where M denotes the STC of each region at each chosen year (i.e., M locations) and N the number of time points. EOF analysis yields M orthogonal spatial basis functions $\phi_k(x)$ such that

$$S_j(t) = \sum_{k=1}^{M} \alpha_k(t)\phi_k(x_j) \ , \tag{3}$$

where α_k is the amplitude of the kth orthogonal mode at time t, and x_j is the location where S_j was observed.

As detailed in Emery and Thomson (2001), the EOF basis functions and time-dependent amplitudes are given respectively by

$$\phi_k(x_j) = [V^k]_j \ , \alpha_k(t) = \sum_{m=1}^{M} S_m(t)[V^k]_m \ , \tag{4}$$

where V^k are eigenvectors of the covariance matrix.

OSD
6, 2831–2859, 2009

3 Results

The Philippine region considered in this analysis is shown in Fig. 2. The SST data for the 5th week of 1985 is shown. To create the binary data, points whose SST are below the threshold (25.1646) are given a value of 0 while SST values greater than the threshold are given the value of 1. Also plotted in the figure are the rectangular areas representative of the six thermal regions.

3.1 STC of the whole Philippines

In Fig. 3, we plot the STC of the weekly Philippine SST from 1985 to 2005 using non-overlapping time slices with thickness 3, 4 and 5 and overlapping slices with thickness 3, 4, 5. For the overlapping case, two consecutive time slices overlap in $N-1$ time points where N is the thickness of the time slice, i.e., if the ith time slice contains the time points T_i, $T_{i+1}, \ldots T_{i+N-1}$, then the next time slice contains T_{i+1}, $T_{i+2}, \ldots T_{i+N}$. The qualitative behavior of the STC using different time slices and moving cubes (including the case for time slice thickness of 5 and cube of dimensions 4 and 5 which are not plotted here) are similar and thus for the succeeding STC calculations in the thermal regions, only non-overlapping time slices of thickness 3 and a moving cube of size 3 are used. To compare the behavior of normal, El Niño and La Niña years, we also indicate in the figure the chosen El Niño years (1987, 1997 and 2002), La Niña (1988, 1998 and 2001) and normal years (1985, 1990, 1993 and 1994). In the figure, El Niño years are highlighted in blue, La Niña in red, normal in green and those which are not highlighted are not selected for analysis.

As seen in the figure, the qualitative behavior of the STC for each year is similar in the sense that the STC is high at the start and end of each year, and low STC (around 0.2) was sustained between weeks 21–42 (roughly May to September). These observations can be explained by the prevailing winds of the Philippines (see discussion below). We also observed that during the transition into the three La Niña years (1988, 1998 and 2001), three of the lowest STC peaks were obtained. The STC of El Niño years, how-

OSD
6, 2831–2859, 2009

ever, do not have clearly distinguishable features from normal years. For example, the highest STC peak was obtained during the transition from normal to El Niño (1986 to 1987) but the second highest STC was obtained during the transition to a normal year (1992 to 1993). Hence we proceed in the next section by computing thermal regions and showing that yearly variations in STC dynamics are obtained in this manner for each region.

3.2 STC of the thermal regions

The clustering methodology yielded six thermal regions whose locations are indicated in Fig. 2. Region 1 is located north of Luzon, Region 2 is located in the northern part of the Philippine Sea, Region 3 is located in the southern part of the Philippine Sea, Region 4 is in the west of the Philippines facing the South China Sea, Region 5 is in the Sulu Sea and Region 6 is south of Mindanao facing the Sulawesi/Celebes Sea.

The spatio-temporal complexity of each region can be summarized by a single STC calculation obtained by moving a $3 \times 3 \times 3$ cube in the area covered by the region and along the whole time dimension (52 weeks times 21 years). The single-STC values are given in Table 4 showing that the STC of Thermal Region 6 stands out. This observation is consistent with the STC time-plots to be discussed below. The density of the 3-D binary data (showing that the density of the 6 regions are similar) and their dimensions are given in Table 4.

Plotting the STC values of the thermal regions for the 21-year period could not reveal the differences in the thermal regions (figure not shown) thus, we plot in Fig. 4 the yearly profiles of STC vs time of each thermal region for three El Niño years (1987, 1997 and 2002), three La Niña years (1988, 1998 and 2001) and four normal (non-ENSO) years (1985, 1990, 1993 and 1994). The plots in Fig. 4 were obtained using non-overlapping slices of thickness 3 and a moving cube of size 3.

Figure 4 shows that Thermal Region 1 (TR1) has the most temporally defined peaks (weeks 15–18 and weeks 42–51) regardless if it is a normal, El Niño or La Niña year. During La Niña years the 1st peak happens earlier at week 15 (mid-April) while dur-

OSD
6, 2831–2859, 2009

ing El Niño the 1st peak happens later during week 18 (early May). For a normal year, the 2nd peak happens early during weeks 42–45 (mid-October to mid-November) while during both El Niño and La Niña years the 2nd peak happens a month later at weeks 45-51 (mid-November until late December).

Thermal Region 2 (TR2) has the 1st peak between weeks 12–21 with the peak appearing earlier during La Niña (late March through April) than in the other years (mid April through May). The 2nd peak happens from October to December reaching a maximum value later during La Niña years (December).

STC is high for normal years at Thermal Region 3 (TR3) but there are 3 distinct peaks during El Niño and 2 peaks during La Niña. The 3 peaks during El Niño happen during weeks 15–18 (mid-April to early May), weeks 33–36 (mid-August to mid-September), and during weeks 48–51 (December). During La Niña, the 1st peak starts earlier at weeks 12–18 (late March to early May), while the last peak also happens during December. There is no middle peak.

For Thermal Region 4 (TR4) there are 2 peaks during normal years, while there are 3 distinct peaks for both El Niño and La Niña years. The 2 peaks during normal years happen on week 15 (mid-April) and a broad high signal from weeks 27–51 (mid-July to the end of the year). During El Niño years the peaks are on week 15; weeks 30–36 (end of July to early September) and week 51 (end of December). For La Niña, the 1st peak happens early on weeks 9–15 (March to mid-April), the 2nd on week 30 (end of July), and the 3rd happens between weeks 42–51 (mid-October to the end of the year).

Thermal Region 5 (TR5) has 2 peaks during normal and La Niña years and 3 peaks during El Niño. For normal years the 1st peak happens during weeks 15–18 (mid-April to early May), while a 2nd broad high signal is seen from weeks 24–45 (mid-June to mid-November). During the El Niño the 1st peak is also during weeks 15–18 while the last peak happens later on week 51 (end of December). There is also a middle peak during weeks 33–36 (mid-August to mid-September). La Niña brings an earlier 1st peak at week 12 (late March) and a last peak at weeks 42–45 (mid-October to mid-November).

OSD

6, 2831–2859, 2009

For Thermal Regions 1–5, 1998 gives a noticeably different STC signal with prolonged very low STC signals that lasted for about 18 weeks from mid-May to mid-October. The low STC started earliest at TR4, followed by TR1, TR5, TR2, and lastly TR3.

Thermal Region 6 (TR6) stands out since we observe higher STC here compared to the other regions and it shows no distinct peaks during any of the years. Overall there is higher variability of the STC at TR6 during normal years.

Thus, Fig. 4 shows that STC analysis applied to the thermal regions yield different signals for the normal, El Niño and La Niña years and are thus effective identifiers of the complexity at this scale.

3.3 EOF analysis of the thermal region STCs

We now use EOF analysis to compare signals for the different thermal regions during normal years, El Niño years and La Niña years. For each thermal region, three EOF computations are made where the number of data sets for the normal year, El Niño and La Niña are 4, 3 and 3, respectively, corresponding to covariance matrices of sizes 4×4, 3×3 and 3×3, respectively. All data sets have 17 time points since non-overlapping slices of thickness 3 are used (i.e., $N = 17$ in Sect. 2.4).

Table 5 summarizes the percentage of the variability of the data set captured by the most dominant EOF mode (which corresponds to the eigenvalue with the maximum absolute value) for each of the 18 calculations. This percentage is computed by taking the ratio $\lambda_{\max} / \left(\sum_{i=1}^{M} \lambda_i \right)$, where λ_i are the eigenvalues of the $M \times M$ covariance matrix. The table shows that except for one data set (Set 11), the dominant mode captures at least 80% of the variability.

The time dependent amplitudes (Eq. 4) of the dominant modes are plotted in Fig. 5. The amplitude of the chosen mode for TR6 clearly stands out from the rest of the thermal regions during the normal years. This difference is less during El Niño and disappears during La Niña years. We also note that the overall range of the amplitudes

OSD
6, 2831–2859, 2009

during the El Niño years are smaller compared to the overall range of the amplitudes during normal and La Niña years. The reduction in amplitude is best seen for TR1 and TR3.

In Fig. 5, we consider an amplitude above 0.5 or below −0.5 as significant. For normal years, TR6 showed the highest occurrence of significant amplitudes, followed by TR3 and then TR4. TR1 had significant amplitudes at weeks 18 and 42–48, while TR5 had significant amplitudes around weeks 42 and 51. TR2 had significant peaks at weeks 15 and 48.

For an El Niño year, only TR6 and TR4 showed significant amplitudes, mostly associated with the months of July to October. For La Niña, the high amplitudes for TR6 disappeared except for week 24. TR4 still had 3 significant amplitudes associated with weeks 15, 27 and 36. The thermal regions TR1, TR2 and TR3 had peaks on the early part of the year but TR1 had a second peak on week 45. The TR5 had no significant peaks during La Niña.

4 Discussion

Here we discuss the prevailing meteorology and oceanography system of the Philippines as it correlates with observations from the STC signals. In particular that: (1) there was a predominant seasonal variation in the yearly STC plots of the Philippine SST data with STC being relatively higher during the start and towards the end of the year, (2) the highest variability of STC values for most regions was found during the inter-monsoon, and (3) the seasonal variation is modified by ENSO events.

The Philippines is under two surface monsoon regimes: (1) the North East monsoons (or *Hanging Amihan*) and the South West monsoons (or *Hanging Habagat*), transitioned by the inter-monsoon season and (2) the North East Trade Wind Regime. There are annual variations as to the onset months for each seasonal regime but in general, NE monsoons happen between November and April while SW monsoons are from June to September. For the purpose of our discussion we refer to the proposed

OSD
6, 2831–2859, 2009

seasonal regimes of Williams et al. (1993) shown in Table 6.

The weeks with relatively higher STC values of the whole Philippines (see Fig. 3) were observed to coincide with the NE monsoons. This monsoon is characterized by strong winds coming from the north-east (see Fig. 2 for a depiction of wind direction). On the other hand, the weeks where low STC were sustained coincided with the SW monsoons, which are characterized by relatively weaker winds coming from the south-west. Thus, at the country level, it is the monsoon winds (and not El Niño or La Niña) that seem to have the largest effect on the spatio-temporal dynamics of the sea surface temperatures.

The NE monsoons may start as early as October, attain maximum strength in January, weaken in March and disappear in April (Williams et al., 1993). From Fig. 4, we observe that Thermal Regions 1 and 2 experience low STC during the start of the year during the normal, El Niño and La Niña years (the STC values are below 0.4 before week 5). Furthermore, we observe that Thermal Regions 3, 4 and 5 experience low STC at the start of the year only during the normal and El Niño years (the STC values of La Niña years before week 5 are above 0.5), with the exception of year 2002 in Thermal Region 3. This region is particularly sensitive to the Pacific and is the first and last one to feel the effects; thus the high value of STC at the start of the 2002 El Niño year may likely be a carryover of the effects of strong La Niña in the previous year. The intervals of high STC experienced by Thermal Regions 1, 2, 3, 4 and 5 (i.e., STC greater than 0.4 from start of the year up to week 15) coincide with the months where the NE monsoons are strongest.

The STC peak in the Philippine-wide annual cycle (Fig. 3) occurs at the peak of NE monsoons when wind from the NE is strongest and the water column is strongly mixed, with plenty of upwelling events near shelves and strong island wakes. The increase in STC is thus an indication of this mixing. It can also be seen that right before the onet of a La Niña, STC is supressed indicating the presence of large stable water masses at the surface.

OSD

6, 2831–2859, 2009

Aside from the monsoons, the Philippines also experiences tradewinds from the east which gain more influence over Philippine water between the monsoons. During the intermonsoon months therefore, the constantly changing wind direction results in mixed SST signals and high variability of STC. This is best seen for Thermal Regions 1, 2 and 3. The trade winds weaken during El Niño while they become stronger during La Niña (Williams et al., 1993). Figure 4 shows that Thermal Regions 1 and 2 are in fact the first to feel the La Niña achieving the first peak of high STC earlier. The more southerly regions (3, 4 and 5) also react distinctively to the trade winds during La Niña even during the NE monsoons.

Thermal Region 6 stands out from the rest since there were sustained high STC throughout most of the year. Our conjecture is that this area is not as affected by the monsoons since topographically induced eddies are a usual occurrence on this part all throughout the year. These eddies mix the sea surface preventing large patches of high SST from forming and thus producing high STC values most of the time.

We also note that for 1998, all the thermal regions had sustained low STC values around weeks 27–39 except for Thermal Region 6. This coincides with the worst coral bleaching event of the world. During this event, Thermal Region 4 had the worst coral bleaching in the Philippines. The low STC values indicate that the temperature was consistently above average, with little spatial heterogeneity, over all the Thermal Regions 1–5.

5 Conclusions

STC was not able to distinguish between El Niño, La Niña and normal years when it was applied to the Philippine SST data but it was able to differentiate between the monsoonal weather experienced by the country every year. When STC was applied to the SST of the thermal regions, we were able to see differences in the STC plots of the El Niño, La Niña and normal years. The STC plots during normal years showed high variability while STC plots during La Niña years showed the least variability. STC

OSD
6, 2831–2859, 2009

was also able to identify that the 1998 La Niña year was different from the other La Niña years since the prolonged repressed STC plots of 1998 stood out in all thermal regions, except in Thermal Region 6.

Among all the thermal regions, the computation of the STC of the 21 year SST data showed that Thermal Region 6 is the most complex in time and in space. STC was able to capture the effect of the usual presence of eddies in Thermal Region 6 by assigning high STC values for this thermal region most of the time. STC was also able to capture the sensitivity of Thermal Regions 2, 3 and 6 to La Niña events and Thermal Region 5 to both La Niña and El Niño events. The complexity signatures of Thermal Regions 1 and 4 are shown to be less variant to ENSO events.

Although STC was applied only to binary data in this paper, the formula for STC can be modified to be able to include application to multi-valued matrices. To do this, one can consider a matrix of n values where each matrix entry depends on the satisfaction of one of n conditions. In addition, we also showed that despite this binary limitation, STC was still able to differentiate between the El Niño, La Niña and normal years when we zoomed in on the thermal regions. This suggests that if ever STC is not able to determine temporal differences from a given data set, one can zoom in on specific areas and explore if STC will be able to present temporal variations at a finer scale. We conclude that the STC measure is thus potentially useful for the analysis of many different types of remotely sensed data in which the objective is to detect and characterize regions of spatio-temporal variability in the environment.

Acknowledgements. The authors would like to thank William Skirving of NOAA-CRW and WB/GEF-RSWG for providing us with the 4 km dataset. We would also like to acknowledge the invaluable assistance of Ms. Eileen Penaflor for the pre-processing of the data. Finally, we express gratitude to Eduardo Mendoza of the University of Munich, Physics Department and Center for Nano-Science for inspiring this inter-disciplinary collaboration.

References

Andrienko, Y. A., Brillantov, N. V., and Kurths, J.: Complexity of two-dimensional patterns, The European Physical Journal, 15, 539–546, 2000. 2833

Atmanspacher, H.: A Semiotic Approach to Complex Systems, in: Aspects of Automatic Text Analysis, edited by: Mehler, A. and Köhler, R., Springer, Berlin, 79–91, 2007. 2837

Bak, P. and Chen, K.: Self-organized criticality, Scientific American, 264, 46–53, 1991. 2837

Banks, H., del Rosario, R., and Tran, H.: Experimental Implementation of POD Based Reduced Order Controllers on Cantilever Beam Vibrations, IEEE Transactions on Control Systems Tech., 10, 717–726, 2002. 2837

Botin, Z. T.: Spatio-Temporal Complexity of the Sea Surface Temperatures of the Philippines, MS Thesis, College of Science, University of the Philippines Diliman, 2009. 2836

Bruno, J. F., Selig, E. R., Casey, K. S., Page, C. A., Willis, B. L., Harvell, C. D., Sweatman, H., and Melendy, A. M.: Thermal Stress and Coral Cover as Drivers of Coral Disease Outbreaks, PloS Biol., 5, e124, 2007. 2832

Buddemeier, R. W., Smith, S. V., Swaney, D. P., Crossland, C. J., and Maxwell, B. A.: Coastal typology: An integrative "neutral" technique for coastal zone characterization and analysis, Estuarine Coastal and Shelf Science, 77, 197–205, 2008. 2837

Emery, W. J. and Thomson, R. E.: Data Analysis Methods in Physical Oceanography: Second and Revised Edition, Elsevier, 2001. 2837, 2838

Glynn, P. W. and D'Croz, L. D.: Experimental Evidence for High Temperature Stress as the Cause of El Niño-Coincident Coral Mortality, Coral Reefs, 8, 181–191, 1990. 2832

Goldenfeld, N.: Lectures on Phase Transitions and the Renormalization Group, Addison-Wesley, Boston, 1992. 2837

Lesser, M. P., Stochaj, W. R., Tapley, D. W., and Shiek, J. M.: Bleaching in Coral Reef Anthozoans: Effects of Irradiance, Ultraviolet Radiation, and Temperature on the Activities of Protective Enzymes against Active Oxygen, Coral Reefs, 8, 225–232, 1990. 2832

MacArthur, R. H.: Fluctuation of Animal Populations and a Measure of Community Stability, Ecology, 36, 533–536, 1955. 2833

National Oceanographic Data Center: 4 km Pathfinder Version 5.0 User Guide, online available at: http://www.nodc.noaa.gov/sog/pathfinder4km/userguide.html, 2008. 2834

Nsakanda, A. L., Price, W. L., Diaby, M., and Gravel, M.: Ensuring Population Diversity in Genetic Algorithm: A Technical Note with Application to the Cell Formation Problem, Eur. J.

Oper. Res., 178, 634–638, 2007. 2833
Parrott, L.: Quantifying the Complexity of Simulated Spatiotemporal Population Dynamics, Ecological Complexity, 2, 175–184, 2005. 2833, 2836
Parrott, L., Proulx, R., and Thibert-Plante, X.: Three dimensional metrics for the analysis of ecological data, Ecological Informatics, 3, 343–353, 2008. 2833, 2836
Peñaflor, E. L., Skirving, W. J., Strong, A. E., Heron, S. F., and David, L. T.: Sea-surface temperature and thermal stress in the Coral Triangle over the past two decades, Coral Reefs, 28(4), 841–850, doi:10.1007/s00338-009-0522-8, 2009. 2832, 2837
Pratchett, M. S., Wilson, S. K., and Baird, A. H.: Declines in the Abundance of Chaetodon Butterflyfishes Following Extensive Coral Depletion, J. Fish. Biol., 69, 1269–1280, 2006. 2832
Reichl, L. E.: A Modern Course in Statistical Physics, 2nd ed., Wiley & Sons, NewYork, 1998. 2837
Strong, A. E., Barrientos, C., Duda, C., and Sapper, J.: Improved Sattelite Techniques for Monitoring Coral Reef Bleaching, Proc 8th International Coral Reef Symposium, Panama City, Panama, 1495–1498, 1996. 2832
Turcotte, D. L.: Fractals and chaos in geology and geophysics, Cambridge University Press, Cambridge, 1997. 2837
Wackerbauer, R., Witt, A., Atmanspacher, H., , Kurths, J., and Scheingraber, H.: A comparative classification of complexity measures, Chaos, Solitons and Fractals, 4, 133–173, 1994. 2833
Williams, F. R., Jung, G. H., and Englebreston, R. E.: Forecasters Handbook for the Philippine Islands and Surrounding Waters, Naval Research Laboratory, Monterey, CA, 1993. 2844, 2845, 2851, 2854

OSD
6, 2831–2859, 2009

Table 1. STC values of each of the thermal regions computed over 21 years (1092 weeks). The density (ratio of non-zero entries in the 3-dimensional matrix over total entries in the 3-dimensional matrix) and dimensions of the matrices are also given.

Thermal Region	STC Value	Density	Dimension of 3-D Binary Matrix
1	0.57	0.57	$26 \times 51 \times 1092$
2	0.64	0.56	$36 \times 56 \times 1092$
3	0.74	0.56	$31 \times 51 \times 1092$
4	0.74	0.56	$41 \times 56 \times 1092$
5	0.76	0.58	$36 \times 56 \times 1092$
6	0.92	0.49	$41 \times 41 \times 1092$

OSD

6, 2831–2859, 2009

Table 2. The sets of data analyzed by EOF and the percentage of the variability of the set captured by the most dominant EOF mode.

Set	Thermal Region	Years (Data Sets)	Variability Captured by dominant mode
1	1	El Niño – 1987, 1997, 2002	95.12%
2	1	La Niña – 1988, 1998, 2001	88.45%
3	1	Normal – 1985, 1990, 1993, 1994	83.19%
4	2	El Niño – 1987, 1997, 2002	86.81%
5	2	La Niña – 1988, 1998, 2001	87.24%
6	2	Normal – 1985, 1990, 1993, 1994	84.35%
7	3	El Niño – 1987, 1997, 2002	92.47%
8	3	La Niña – 1988, 1998, 2001	86.21%
9	3	Normal – 1985, 1990, 1993, 1994	88.25%
10	4	El Niño – 1987, 1997, 2002	92.93%
11	4	La Niña – 1988, 1998, 2001	76.03%
12	4	Normal – 1985, 1990, 1993, 1994	92.64%
13	5	El Niño – 1987, 1997, 2002	92.74%
14	5	La Niña – 1988, 1998, 2001	87.78%
15	5	Normal – 1985, 1990, 1993, 1994	93.17%
16	6	El Niño – 1987, 1997, 2002	95.78%
17	6	La Niña – 1988, 1998, 2001	93.84%
18	6	Normal – 1985, 1990, 1993, 1994	95.35%

OSD
6, 2831–2859, 2009

Table 3. Seasons of the Philippines, adapted from Williams et al. (1993).

Inter-monsoon	Oct–Nov
NE Monsoon formation	Sep–mid Oct
NE Monsoon or Trade Wind	Nov–Apr
North Pacific Trade Wind	Mar
Intermonsoon	Apr–May
SW Monsoon formation	Mar–Jun
SW Monsoon	Jun–Oct

OSD

6, 2831–2859, 2009

Table 4. STC values of each of the thermal regions computed over 21 years (1092 weeks). The density (ratio of non-zero entries in the 3-dimensional matrix over total entries in the 3-dimensional matrix) and dimensions of the matrices are also given.

Thermal Region	STC Value	Density	Dimension of 3-D Binary Matrix
1	0.57	0.57	$26 \times 51 \times 1092$
2	0.64	0.56	$36 \times 56 \times 1092$
3	0.74	0.56	$31 \times 51 \times 1092$
4	0.74	0.56	$41 \times 56 \times 1092$
5	0.76	0.58	$36 \times 56 \times 1092$
6	0.92	0.49	$41 \times 41 \times 1092$

OSD

6, 2831–2859, 2009

Table 5. The sets of data analyzed by EOF and the percentage of the variability of the set captured by the most dominant EOF mode.

Set	Thermal Region	Years (Data Sets)	Variability Captured by dominant mode
1	1	El Niño – 1987, 1997, 2002	95.12%
2	1	La Niña – 1988, 1998, 2001	88.45%
3	1	Normal – 1985, 1990, 1993, 1994	83.19%
4	2	El Niño – 1987, 1997, 2002	86.81%
5	2	La Niña – 1988, 1998, 2001	87.24%
6	2	Normal – 1985, 1990, 1993, 1994	84.35%
7	3	El Niño – 1987, 1997, 2002	92.47%
8	3	La Niña – 1988, 1998, 2001	86.21%
9	3	Normal – 1985, 1990, 1993, 1994	88.25%
10	4	El Niño – 1987, 1997, 2002	92.93%
11	4	La Niña – 1988, 1998, 2001	76.03%
12	4	Normal – 1985, 1990, 1993, 1994	92.64%
13	5	El Niño – 1987, 1997, 2002	92.74%
14	5	La Niña – 1988, 1998, 2001	87.78%
15	5	Normal – 1985, 1990, 1993, 1994	93.17%
16	6	El Niño – 1987, 1997, 2002	95.78%
17	6	La Niña – 1988, 1998, 2001	93.84%
18	6	Normal – 1985, 1990, 1993, 1994	95.35%

OSD
6, 2831–2859, 2009

Table 6. Seasons of the Philippines, adapted from Williams et al. (1993).

Inter-monsoon	Oct–Nov
NE Monsoon formation	Sep–mid Oct
NE Monsoon or Trade Wind	Nov–Apr
North Pacific Trade Wind	Mar
Intermonsoon	Apr–May
SW Monsoon formation	Mar–Jun
SW Monsoon	Jun–Oct

OSD
6, 2831–2859, 2009

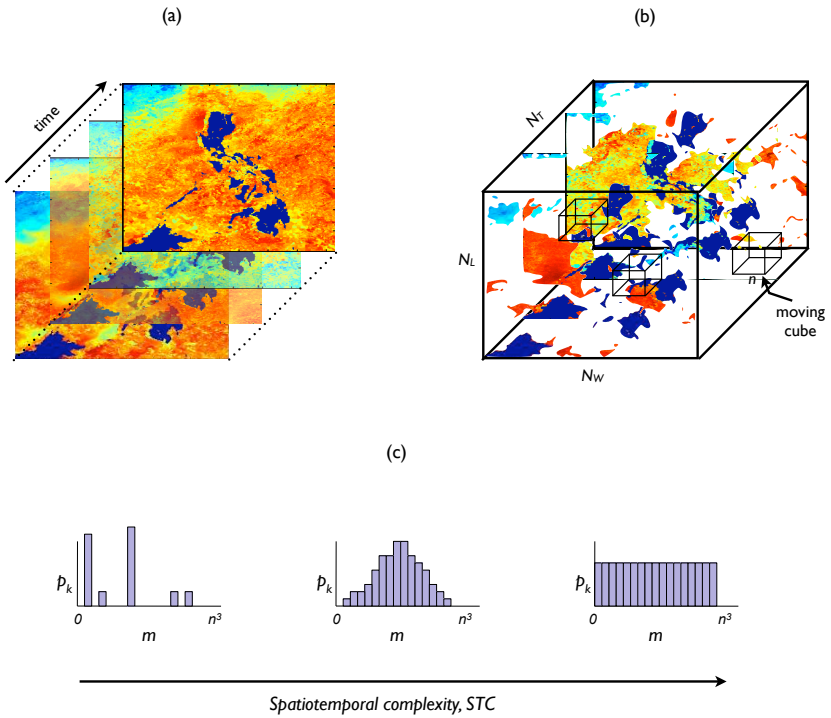

Fig. 1. Schematic of the spatio-temporal complexity analysis: **(a)** the series of raster-based sea surface temperature (SST) images are stacked into a 3-D space-time matrix. **(b)** A threshold temperature is applied to generate a binary matrix, in which all cells below the threshold have zero values (shown here as empty cells). An $n \times n \times n$ moving cube is placed at successive locations in the space-time matrix like a sliding window. At each location, the number of non-zero entries (m) in the cube is noted. The relative frequency, p_k, that each occupancy level, m, is observed is calculated. **(c)** Frequency histograms of p_k versus m. A highly uneven histogram (left) is indicative of ordered space-time dynamics and gives a low value of spatio-temporal complexity (STC). A bell-shaped histogram (middle) is indicative of a random distribution of non-zero entries in the space-time matrix and gives an intermediate value of STC. A perfectly even histogram (right) arises when the space-time matrix is populated with patches of all different sizes and shapes and gives a maximal value of STC.

OSD
6, 2831–2859, 2009

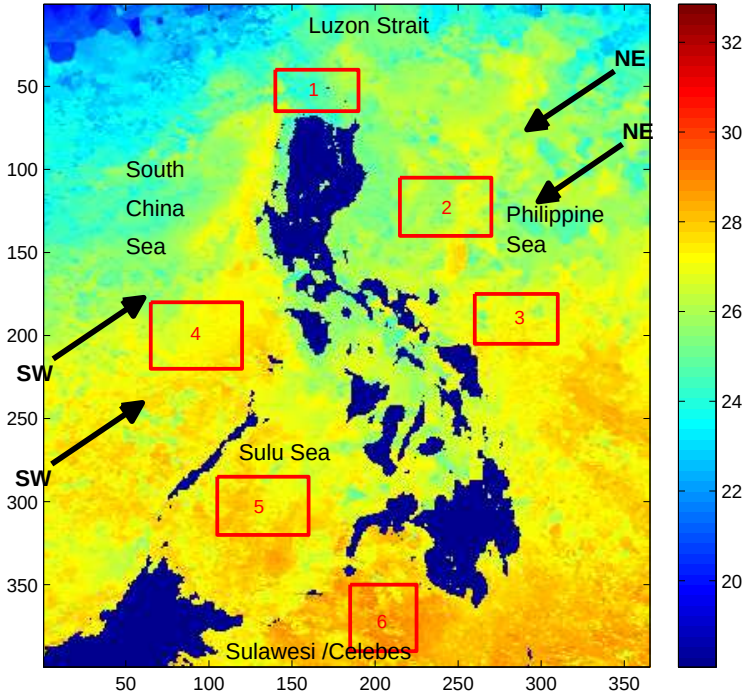

Fig. 2. The matrix from SST data taken on the fifth week of 1985 during the NE monsoon season. The arrows indicate the direction of the prevailing winds during NE and SW monsoon (not scaled to indicate wind strength). The location of the six thermal regions are indicated in boxes.

OSD

6, 2831–2859, 2009

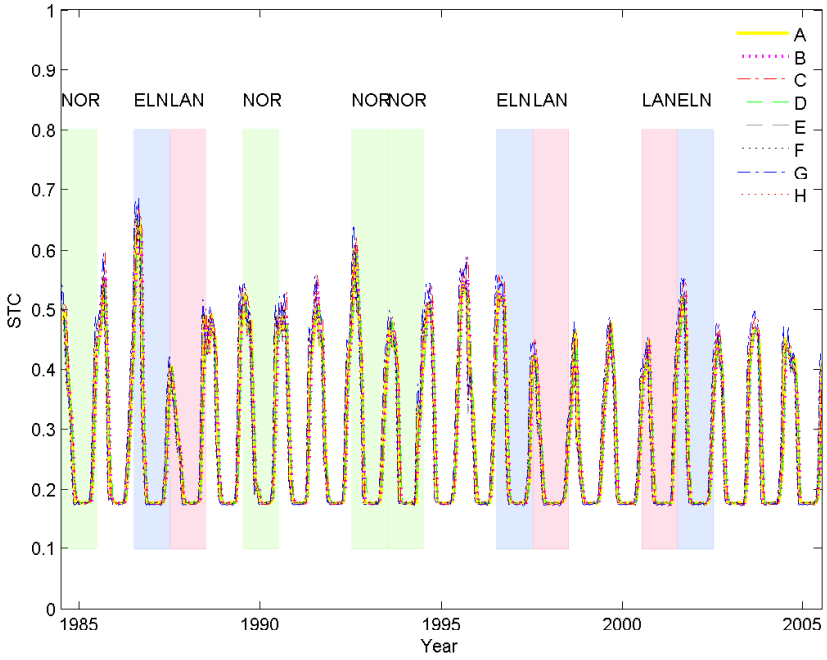

Fig. 3. The STC of the Philippine SST from 1985 to 2005. **A** Non-overlapping: slice thickness $N = 3$, moving cube dimension $n = 3$; **B** Non-overlapping: $N = 4$, $n = 3$; **C** Non-overlapping: $N = 4$, $n = 4$; **D** Non-overlapping: $N = 5$, $n = 3$; **E** Overlapping: $N = 3$, $n = 3$; **F** Overlapping: $N = 4$, $n = 3$; **G** Overlapping: $N = 4$, $n = 4$; **H** Overlapping: $N = 5$, $n = 3$. Results with non overlapping and overlapping slice thickness of 5 and cube dimensions of 4 and 5 are similar and hence are not plotted. NOR: normal years, ELN: El Niño years, LAN: La Niña. The non-highlighted years are not selected for analysis.

OSD
6, 2831–2859, 2009

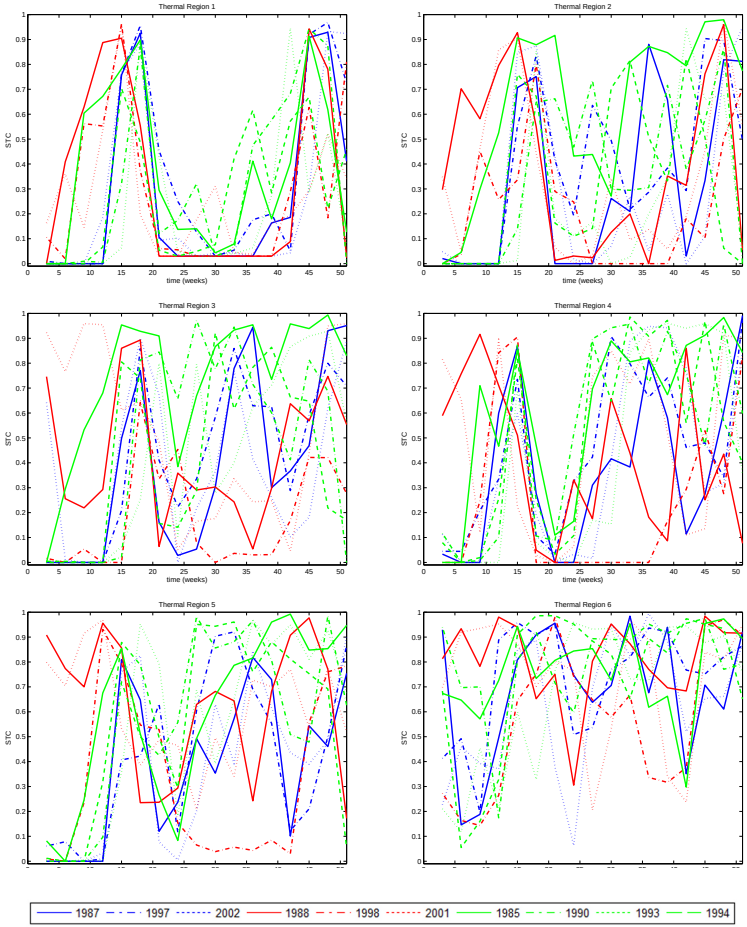

Fig. 4. STC of the six thermal regions for each of the chosen years: 3 El Niño (1987, 1997, 2002), 3 La Niña (1988, 1998, 2001) and 4 normal years (1985, 1990, 1993, 1994). All line styles have the same meaning as in the legend box; blue: El Niño, red La Niña, green: normal.

OSD

6, 2831–2859, 2009

Spatio-Temporal Complexity Analysis of Philippine SST

Z. T. Botin et al.

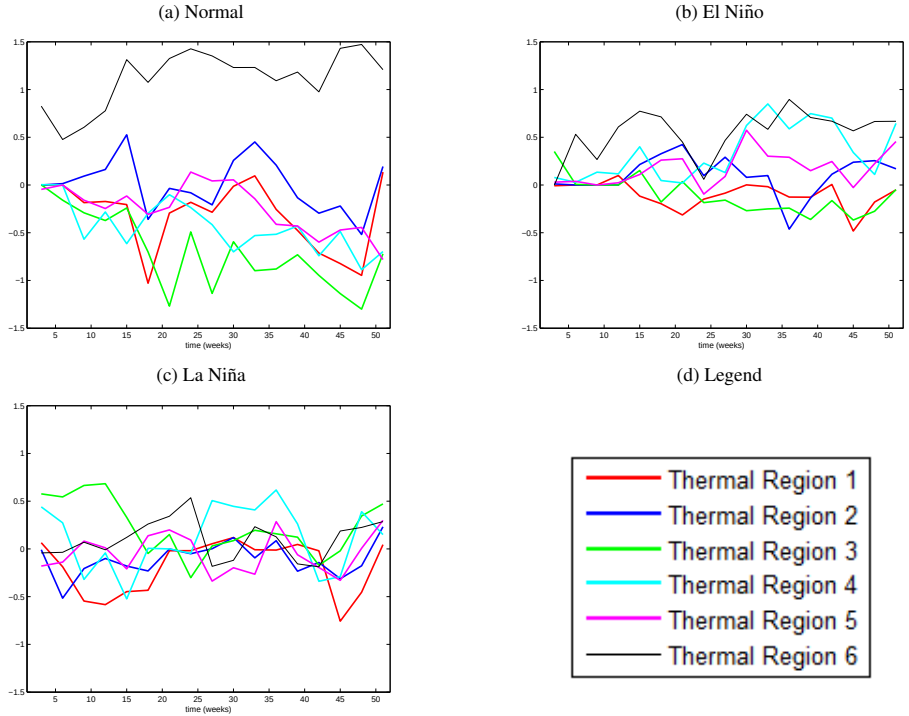

Fig. 5. The time-dependent EOF amplitudes of the dominant modes for each set of data **(a–c)**. All line styles are described in the legend box **(d)**.

OSD
6, 2831–2859, 2009